Northeast Gulf Science

Volume 12
Number 1 *Number 1*

Article 1

11-1991

Numerical Computations of a Two-Layer Model for Estuaries

Kang-Ren Jin
Mississippi State University

Donald C. Raney
University of Alabama

DOI: 10.18785/negs.1201.01

Northeast Gulf Science Vol. 12, No. 1 November 1991 p. 1-15

NUMERICAL COMPUTATIONS OF A TWO-LAYER MODEL FOR ESTUARIES

Kang-Ren Jin
Department of Civil Engineering
Mississippi State University, MS 39762
and
Donald C. Raney
Department of Mechanical Engineering
The University of Alabama, AL 35487-0276

ABSTRACT: The research described in this paper is aimed at improving the predictive capability of numerical models for estuarine circulation. An improved two-layer model has been developed, which is applicable to the entire estuary including areas near the river mouth and the estuary inlet. This model is applied to Apalachicola Bay, Florida. The calibration and verification of the numerical model is accomplished with available prototype data. The horizontal density gradient terms have been added to the model and provide significantly improved salinity predictions near the river mouths. A theoretical approach to the internal wave boundary condition has been developed in this two-layer model.

Since early times, estuaries and river mouths have been utilized in many ways, for example, as fishery ports, navigation harbors, suppliers of water for industries, etc. Recently, with a growth of utilization of the estuaries and river mouths, environmental problems have attracted public attention. Saline intrusion has long been recognized as a difficulty to agriculture, water supply systems and certain industries. Sewage and waste along with oil spills have more recently become of utmost concern as a result of possible impact on human health.

Over the past 20 years, numerical modeling of estuaries has become an established tool for scientist. A variety of numerical models are available based on both finite difference and finite element formulations of the basic governing equations: for example, two-dimensional depth averaged models (Raney, Huang, and Urgun, 1987), three-dimensional hydrodynamic models (Davies, 1981), two-layer shallow-water models (Vreugdenhil, 1979), and two-layer hydrodynamic and salinity models (Jin and Raney, 1989). The two-layer simulation model is potentially one of the most accurate and efficient tools for addressing circulation problems in estuaries.

A two-layer hydrodynamic and salinity model is used to examine the flow parameters in the upper and lower layers of a stratified estuary and to compare the difference between these two layers. This research lays the foundation for the development of an improved system for numerical simulation of estuarine hydrodynamics and salinity.

Pritchard (1971) indicates that density gradients are important in the James Estuary. Smith and Cheng (1987) applied horizontal density gradients in a model of Suisum Bay, California. Their papers illustrate that the exclusion of horizontal density gradient terms would lead to overestimation of freshwater inflow for a fixed set of model boundary conditions. Recent experiences with hydrodynamic salinity models have demonstrated that obtaining an accurate salinity distribution in an estuary may require consideration of horizontal density gradients (Raney and

Jin, 1988). The importance of density gradients in ocean circulation is well established but these terms have often been neglected in estuaries.

The horizontal density gradients have been formulated in a two-layer hydrodynamic and salinity model. The numerical model is applied to Apalachicola Bay, Florida (Figure 1), both with and without horizontal density gradient terms included. Resulting salinity distributions in the bay are presented in a graphical format, and comparisons are made to quantify the effect of these terms. The model has been calibrated and verified using prototype data collected in September 1983 and March 1984, respectively by Continental Shelf Associates, Inc. and the U.S. Army Corps of Engineers, Mobile District (USCEM). Sufficient prototype data are available to demonstrate that the numerical model reproduces the behavior of the bay system when subjected to variations in tidal elevation, salinity, river inflow, and wind boundary conditions.

THE MODELING SYSTEMS AND BASIC EQUATIONS

The hydrodynamic equations used in this model are derived from the classical Navier-Stokes equations and the continuity equation in a Cartesian coordinate system. For turbulent flow in Cartesian coordinate, these equations take the form:

$$\rho\left(u\frac{\partial u}{\partial x}+v\frac{\partial u}{\partial y}+w\frac{\partial u}{\partial z}+\frac{\partial u}{\partial t}\right)-\rho fv=-\frac{\partial p}{\partial x}+k\left(\frac{\partial^2 u}{\partial x^2}+\frac{\partial^2 u}{\partial y^2}+\frac{\partial^2 u}{\partial z^2}\right) \quad (1)$$

$$\rho\left(u\frac{\partial v}{\partial x}+v\frac{\partial v}{\partial y}+w\frac{\partial v}{\partial z}+\frac{\partial v}{\partial t}\right)+\rho fu=-\frac{\partial p}{\partial y}+k\left(\frac{\partial^2 v}{\partial x^2}+\frac{\partial^2 v}{\partial y^2}+\frac{\partial^2 v}{\partial z^2}\right) \quad (2)$$

$$\rho\left(u\frac{\partial w}{\partial x}+v\frac{\partial w}{\partial y}+w\frac{\partial w}{\partial z}\frac{\partial w}{\partial t}\right)-\rho g=-\frac{\partial p}{\partial z}+k\left(\frac{\partial^2 w}{\partial x^2}+\frac{\partial^2 w}{\partial y^2}+\frac{\partial^2 w}{\partial z^2}\right) \quad (3)$$

$$\frac{\partial p}{\partial t}+\frac{\partial(\rho u)}{\partial x}+\frac{\partial(\rho v)}{\partial y}+\frac{\partial(\rho w)}{\partial z}=0 \quad (4)$$

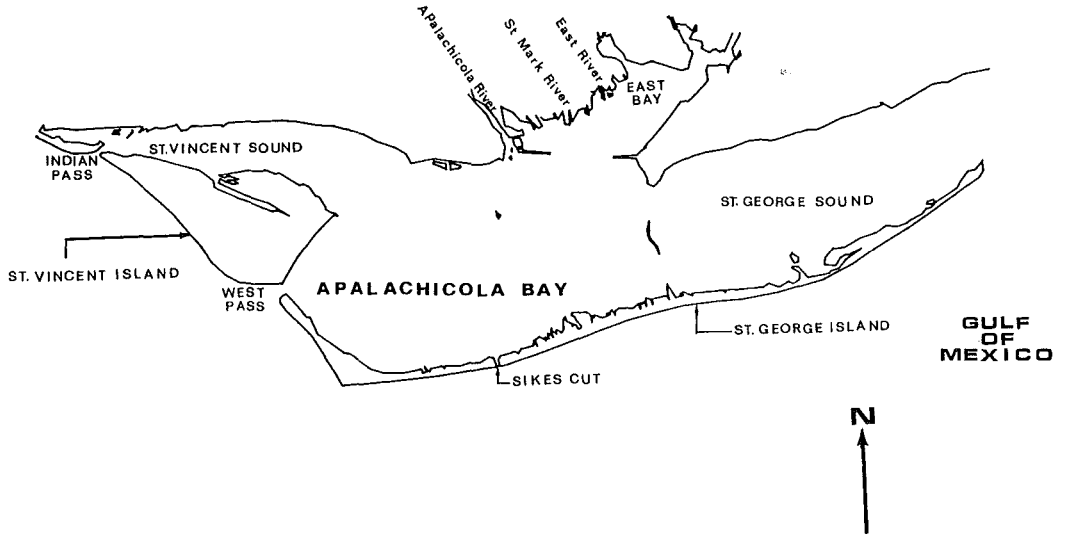

Figure 1. Apalachicola Bay System: Includes Apalachicola Bay, St. Vincent Sound, East Bay, St. George Sound.

DOI: 10.18785/negs.1201.01

The usual two-layer hydrodynamic equations are obtained by assuming: that the fluid of each layer is incompressible and homogeneous; that vertical accelerations of the fluid of each layer are negligible; and the horizontal flow is reasonably uniform over the fluid depth of each layer. The three-dimensional equations are then integrated over the fluid depth of each layer and forced to satisfy the appropriate boundary conditions. The lower layer depth is from the estuary bottom to the interface between the two layers. The upper layer depth is from the interface to the water surface. The interface location is defined at d_2, and $d_2 = h_2 + \eta_2$ as shown in Figure 2.

Relative to the coordinate system in Figure 2, the model differential equations become:

Upper Layer
Continuity Equation:

$$\frac{\partial \eta_1}{\partial t} - \frac{\partial \eta_2}{\partial t} + \frac{\partial (U_1 d_1)}{\partial x} + \frac{\partial (V_1 d_1)}{\partial y} = 0 \qquad (5)$$

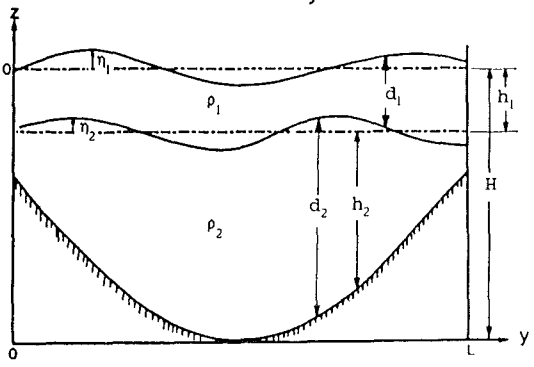

Figure 2. Cartesian Coordinate System for a Two-Layer Hydrodynamic Model.

Momentum Equations:

$$\frac{\partial U_1}{\partial t} + U_1\frac{\partial U_1}{\partial x} + V_1\frac{\partial U_1}{\partial y} = fV_1 - g\frac{\partial \eta_1}{\partial x} + \frac{\tau_{wind)x}}{\rho_1 d_1} - \frac{\tau_{inter)x}}{\rho_1 d_1} + K\left(\frac{\partial^2 U_1}{\partial x^2} + \frac{\partial^2 U_1}{\partial y^2}\right) \quad \ldots\ldots\ldots \text{x-direction} \qquad (6)$$

$$\frac{\partial V_1}{\partial t} + U_1\frac{\partial V_1}{\partial x} + V_1\frac{\partial V_1}{\partial y} = -fU_1 - g\frac{\partial \eta_1}{\partial y} + \frac{\tau_{wind)y}}{\rho_1 d_1} - \frac{\tau_{inter)y}}{\rho_1 d_1} + K\left(\frac{\partial^2 V_1}{\partial x^2} + \frac{\partial^2 V_1}{\partial y^2}\right) \quad \ldots\ldots\ldots \text{y-direction} \qquad (7)$$

Lower Layer
Continuity Equation:

$$\frac{\partial \eta_2}{\partial t} + \frac{\partial (U_2 d_2)}{\partial x} + \frac{\partial (V_2 d_2)}{\partial y} = 0 \qquad (8)$$

Momentum Equations:

$$\frac{\partial U_2}{\partial t} + U_2\frac{\partial U_2}{\partial x} + V_2\frac{\partial U_2}{\partial y} = fV_2 - g\frac{\rho_1}{\rho_2}\frac{\partial \eta_1}{\partial x} - g\frac{\partial \eta_2}{\partial x}\left(1 - \frac{\rho_1}{\rho_2}\right) + \frac{\tau_{inter)x}}{\rho_2 d_2} - \frac{\tau_{bottom)x}}{\rho_2 d_2} + K\left(\frac{\partial^2 U_2}{\partial x^2} + \frac{\partial^2 U_2}{\partial y^2}\right) \quad \ldots\ldots\ldots \text{x-direction} \qquad (9)$$

$$\frac{\partial V_2}{\partial t} + U_2\frac{\partial V_2}{\partial x} + V_2\frac{\partial V_2}{\partial y} = fU_2 - g\frac{\rho_1}{\rho_2}\frac{\partial \eta_1}{\partial y} - g\frac{\partial \eta_2}{\partial y}\left(1 - \frac{\rho_1}{\rho_2}\right) + \frac{\tau_{inter)y}}{\rho_2 d_2} - \frac{\tau_{bottom)y}}{\rho_2 d_2} + K\left(\frac{\partial^2 V_2}{\partial x^2} + \frac{\partial^2 V_2}{\partial y^2}\right) \quad \ldots\ldots\ldots \text{y-direction} \qquad (10)$$

Additional equations are necessary to represent the stress condition at the fluid surface, bottom and interface between the two layers (Liu and Leendertse, 1979).

Interfacial stress:
in the x direction:

$$\frac{\tau_{inter)x}}{\rho_1} = \nu\frac{(U_1 - U_2)}{0.5(d_1 + d_2)}\left\{\left[\frac{(U_1 - U_2)}{0.5(d_1 + d_2)}\right]^2 + \left[\frac{(V_1 - V_2)}{0.5(d_1 + d_2)}\right]^2\right\}^{1/2} \qquad (11)$$

Bottom stress:
in the x direction:

$$\frac{\tau_{bottom)x}}{d_2\rho_2} = gU_2\frac{(U_2^2 + V_2^2)^{1/2}}{d_2 c^2} \qquad (12)$$

Wind stress:

$$\frac{\tau_{wind)}}{\rho_w} = \frac{2.15 c_d \rho_a W_\infty^2}{\rho_w}$$

$$c_d \cong 0.0015 \qquad (13)$$

Where,

- c : Chezy Coefficient
- c_d : Drag Coefficient
- d : Total Depth of the Layer
- f : Coriolis Parameter
- g : Gravitational Acceleration
- h : Depth of the Layer
- K : Kinematic Eddy Viscosity
- k : Eddy Viscosity
- p : Pressure

t : Time
U, V, W : Mean Velocity Components in the x, y, z Direction
u, v, w : Velocity Components in the x, y, z Direction
x, y, z : Rectangular Coordinate Variables
η : Vertical Deviation of each layer
ν : Coefficient of Interfacial Friction
p : Density
p_a : Density of Air
p_w : Density of Fresh Water
τ_{bottom} : Bottom Stress
τ_{inter} : Interfacial Stress
τ_{wind} : Wind Stress

Subscripts 1 and 2 represent the upper and lower layers.

The conservation of salt equation can be expressed as:

$$\frac{\partial(dS)}{\partial t}+\frac{\partial(duS)}{\partial x}+\frac{\partial(dvS)}{\partial y}-\frac{\partial(dD_x\frac{\partial S}{\partial x})}{\partial x}-\frac{\partial(dD_y\frac{\partial S}{\partial y})}{\partial y}-d\dot{S}=0 \qquad (14)$$

In this equation, S is salinity, and d is total depth of each layer. D_x and D_y are the mixing coefficients of salt.

ADDITION OF SALINITY GRADIENT TERM

The salinity equation and hydrodynamic equation are coupled through horizontal density gradient terms. These terms for the upper layer can be approximated as a salinity gradient (Raney and Jin, 1988), then;

$$\frac{1}{p_1}\frac{\partial p}{\partial x}=g\frac{\partial \eta_1}{\partial x}+\underline{\frac{1g}{2p_1}(d_1)\left[\frac{\partial p_1}{\partial S}\right]\frac{\partial S}{\partial x}} \qquad (15)$$

$$\frac{1}{p_1}\frac{\partial p}{\partial y}=g\frac{\partial \eta_1}{\partial y}+\underline{\frac{1g}{2p_1}(d_1)\left[\frac{\partial p_1}{\partial S}\right]\frac{\partial S}{\partial y}} \qquad (16)$$

In a similar manner, the density gradient terms can be obtained for the lower layer. The variation of density with salinity is a known physical property. Thus, the horizontal salinity gradient terms can be represented by adding the underlined terms to previous model equations.

BOUNDARY CONDITIONS

The boundary conditions for this two-layer model are open boundaries and water-land boundaries. For the water-land boundaries, the assumption is that of "no flow" normal to the boundary. Open boundaries define the computational cell rows or columns exiting the grid. At these boundaries water levels or flow rates are prescribed as functions of location and time for both layers.

For the lower layer, the elevation boundary condition is an internal wave. Yoshida and Kashiwamura (1976) describe the mechanism of the two-layer flow which varies in response to the tide with an internal wave driving the lower layer. If one expresses the tidal elevation at the upper layer boundary by

$$\eta_1=A\cos(\sigma t+e) \qquad (17)$$

where, A is constant and $e \ll 1$. Then, the approximate form for the internal wave applied to the lower layer can be expressed as

$$\eta_2=(1-\frac{gh_1}{C_{s,i}^2})(b_0+b_1t+b_2t^2+b_3{}^3t+b_4{}^4t+b_5{}^5t+b_6{}^6t) \qquad (18)$$

where $C^2_{s,i}$ is a propagation velocity of the wave.

$$C^2_{s,i}=\frac{g(d_1+d_2)\pm g\sqrt{(d_1+d_2)^2-4ed_1d_2}}{2}. \qquad (19)$$

The polynomial coefficients b_0, b_1, b_2, b_3, b_4, b_5, and b_6 can be determined by curve fitting techniques using a non-linear least square algorithm. Figure 3 illustrates the relationship between an upper layer tidal

DOI: 10.18785/negs.1201.01

boundary condition and the related internal wave applied as a boundary condition to the lower layer.

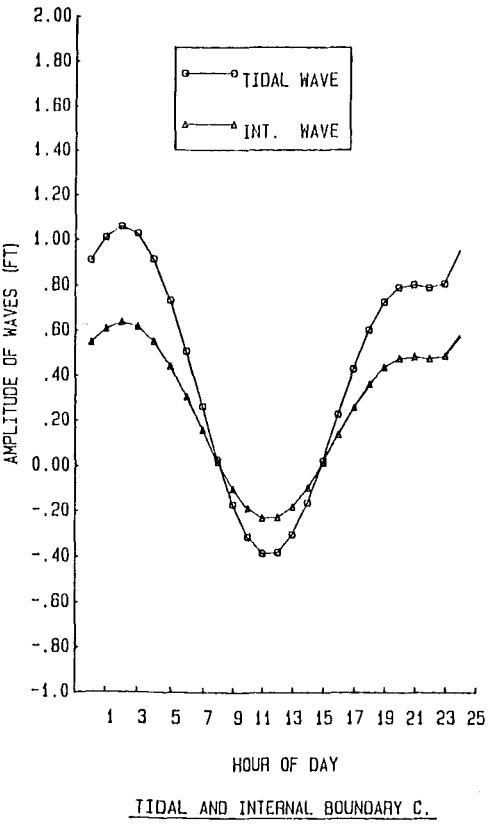

Figure 3. Tidal and Internal Wave Boundary Conditions.

SOLUTION TECHNIQUE

To solve the governing equations, a finite difference approximation of the equations (Roache 1972) and an Alternating Direction Implicit technique (Anderson, Tannehill and Pletcher 1984) are employed. The solution scheme is similar to that proposed by Leendertse (1970, 1971). A space-staggered scheme (Raney, Huang, and Urgun, 1987) is used in which velocities, water-level displacement, salinity, Chezy coefficient, and total water depth are defined at different locations within a grid cell as shown in Figure 4. Central finite differences are used for evaluating all derivatives in the governing equations.

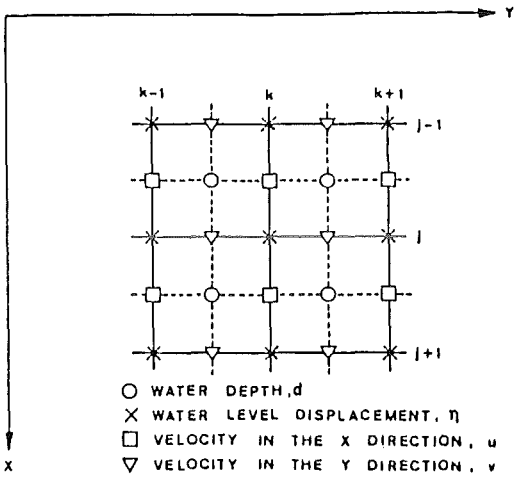

Figure 4. Grid System and Variable Definition Locations.

A high resolution numerical model is desirable with particular emphasis on areas near passes, channels, and other critical features. This is accomplished by applying a smoothly varying grid technique (Wanstrath, Whitaker, Reid, and Vastand 1976).

APALACHICOLA BAY SYSTEM

The test case for this model is the Apalachicola Bay System. Situated on the Florida Panhandle, the Apalachicola Bay System consists of a barrier island contained estuary system. The principal embayment is Apalachicola Bay, bounded by St. Vincent Sound to the west, East Bay to the north, and St. George Sound to the east. These waters comprise an integral estuarine system illustrated in Figure 1.

The approximate dimensions of the Apalachicola Bay System are listed as follows,

	Length (km)	Width (km)	Area (km²)
St. Vincent Sound	14.49	3.22	46.66
East Bay	8.05	4.83	44.07
St. George Sound	17.71	6.44	124.42
Apalachicola Bay	19.32	9.66	199.59

St. Vincent and St. George are barrier islands separating the embayment from the Gulf of Mexico. Access to the Gulf of

Mexico is provided by Indian Pass, West Pass, Sikes Cut, and the northeast end of St. George Island. All of the openings are natural except Sikes Cut. Sikes Cut was dredged across St. George Sound in 1954. The bay system is very shallow with an average depth of 2.44 meter.

The finite difference grid was constructed using a 1:48,000 scale nautical chart. The chart was based upon a bathymetric survey made during September 1983 and March 1984. Bathymetric data were digitized and the best average depth was calculated for each finite difference cell. The Manning *n* friction values from bottom materials (mud, sand, weeds, etc.) were also digitized and interpolated in a similar manner.

The resulting finite difference grid was 82×50 cells for a total of 4100 cells. The geometry for the finite difference cells is shown in Figure 5. Smaller cells were used in areas near passes opening to the Gulf of Mexico, near the Gulf Intracoastal Waterway Channel, and near the inner bar channel. Similarly, in areas where the bay geometry or depths were changing rapidly, or other critical features exist, smaller cells were also used. Larger cells were used in East Bay and other areas of the bay where geometry and bathymetry were reasonably simple or constant.

At all computational boundary openings to the Gulf of Mexico, a time dependent tidal and salinity boundary condition was specified. At the river inflows, volumetric flow rate and salinity boundary conditions were specified. The time dependent freshwater input into the bay was modeled by Apalachicola River, St. Marks River, and East River inflows. A wind shear stress based upon the time varying wind velocity was applied to each finite difference cell.

MODEL CALIBRATION AND VERIFICATION

During two 30-day periods, prototype data from Apalachicola Bay System were collected for calibration and verification of the numerical model. Velocity, salinity, and bathymetric data were collected by Continental Shelf Associates, Inc. while the National Oceanic and Atmospheric Administration, National Ocean Service

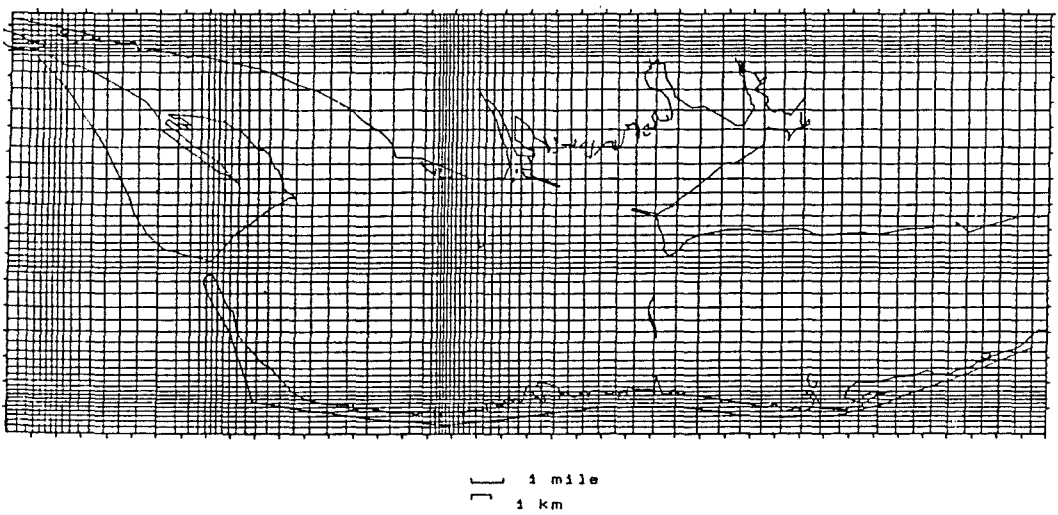

Figure 5. Finite Difference Grid in Apalachicola Bay, Florida.

DOI: 10.18785/negs.1201.01

(NOS) provided the wind and tidal data. Data on fresh water inflow into the bay for the time period of interest were obtained from the U.S. Department of Interior, Geological Survey (USGS). The data locations are indicated as SG1, SG2 . . . SG10 in Figure 5. In addition, the USCEM with the assistance of the USGS and Florida Department of Environmental Regulation, collected salinity data for 24-hour periods during September 14-15, 1983, and March 8-9, 1984. The data locations are indicated as G1, G2 . . . G9 in Figure 6.

The time period September 14-15, 1983 was used as the calibration condition. Appropriate bathymetric and bottom friction data were determined for each finite difference cell of the model. Prototype surface elevation and salinity data were applied as boundary conditions at each computational boundary of the model opening to the Gulf of Mexico. Initial conditions were established for the model and the model was allowed to "warm-up" for a period of time prior to the actual period of calibration. The warm-up period is necessary to allow time for the model to minimize errors associated with incorrect starting conditions. After allowing the model to run for the calibration period, model results were compared with prototype data. Model parameters (friction, depths, diffusivity, etc.) and initial conditions were adjusted appropriately and the model rerun. This process was continued until the model produced results which agreed with prototype data within an acceptable degree of accuracy. The range of the Manning "n" friction coefficient was 0.023-0.03. Van Der Kreeke (1988) discussed dispersion coefficients and the variation in directions parallel and perpendicular to the main current direction. Values predicted by existing formula are shown to vary widely and yield at best an order of magnitude approximation. In this study, a constant value of 15 ft²/sec was used in both x and y directions. The range of the depth is 0.5-7.1 meter, but the average depth is about 2.44m. The Chezy coefficients are calculated from the Manning "n" friction values. The initial condition of salinity was determined for each finite difference cell by interpolating among the available prototype data. The salinity output during initial phases of the calibration process (Raney, Huang, and Urgun 1987).

Simulation results are presented after the numerical results have stabilized

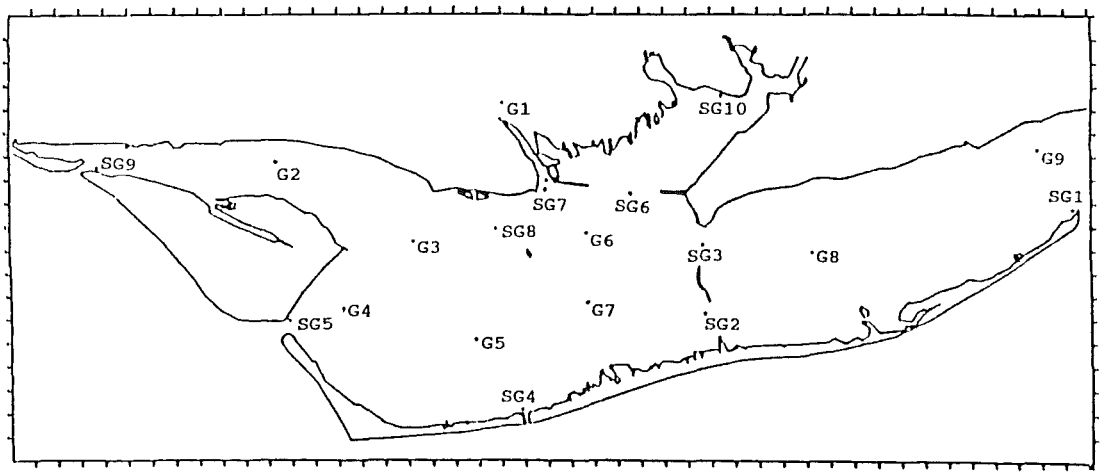

Figure 6. Prototype Data Collection Stations in Apalachicola Bay System.

for each cycle. For this study, modeling results are presented after three tidal cycles. Some calibration results at gage point locations for the two-layer hydrodynamic salinity model run are presented in Figures 7 thru 21. Results are presented

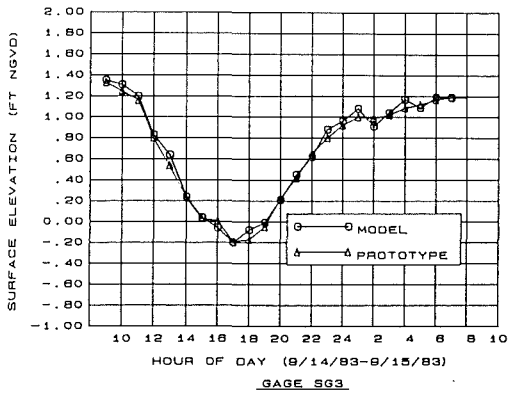

Figure 7. Surface Elevation at Station SG3 for Calibration Condition.

for calculations both with and without horizontal density gradient terms. The surface elevation and velocity results are not changed significantly by the addition of the horizontal density gradient terms. Thus, surface elevation and velocity results are presented only for the conditions without density gradient terms. There are very good agreement of surface elevation and velocity between prototype data and numerical result. For example,

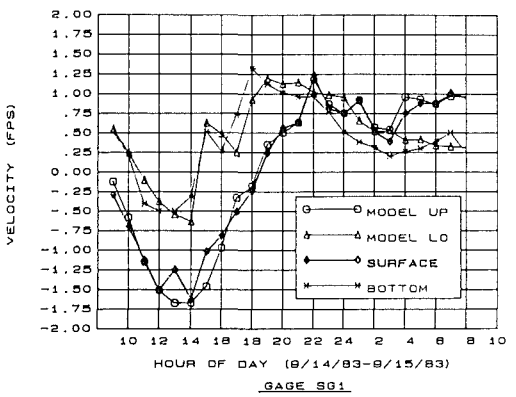

Figure 9. Velocity at Station SG1 for Calibration Condition.

Figures 7 and 8 present the surface elevation without horizontal density gradient terms. The average difference is about 1.8 cm. Velocities without horizontal density gradient terms are presented in Figures 9 and 10. The average difference

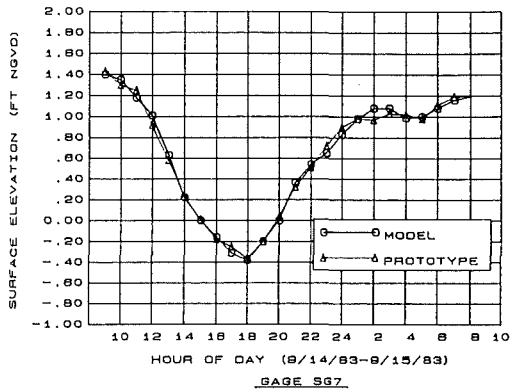

Figure 8. Surface Elevation at Station SG7 for Calibration Condition.

is about 7 cm/sec. Salinity results with and without horizontal density gradient terms are presented in Figures 11 thru 13. In Figures 9 and 10, "MODEL UP" and "MODEL LO" are the model velocity results for the upper and lower layers without the horizontal density gradient terms. The curves labeled "SURFACE", "BOTTOM", and "MIDDEPTH" are prototype data in Figures 9 thru 13. "MODEL 1 UP" is the model salinity results for the

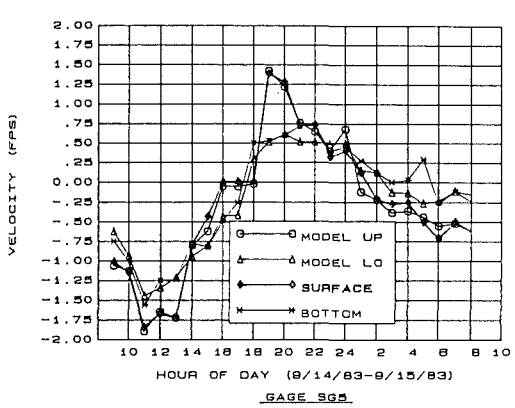

Figure 10. Velocity at Station SG5 for Calibration Condition.

DOI: 10.18785/negs.1201.01

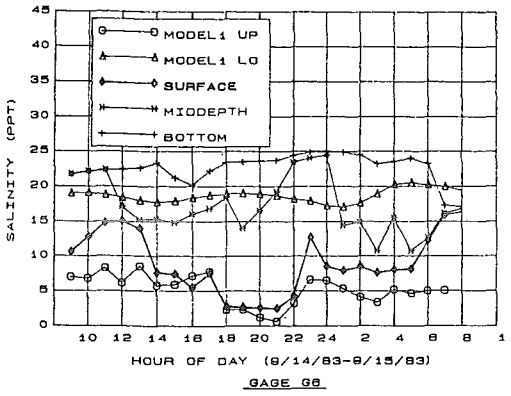

Figure 11A. Salinity at Station G6 of MODEL 1 for Calibration Condition.

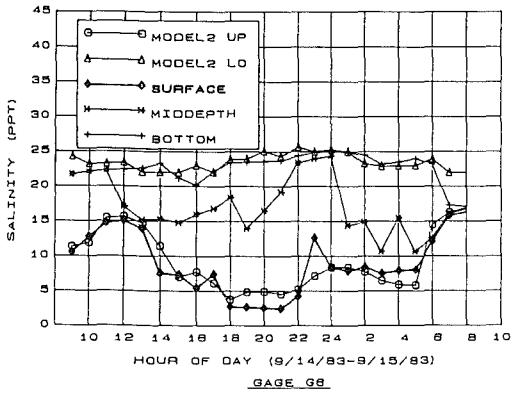

Figure 11B. Salinity at Station G6 of MODEL 2 for Calibration Condition.

upper layer without the horizontal density gradient terms. "MODEL 1 LO" is the model salinity results fo the lower layer without the horizontal density gradient terms. "MODEL 2 UP" is the model salinity results for the upper layer with the horizontal density gradient terms. "MODEL 2 LO" is the model salinity results for the lower layer with the horizontal density gradient terms.

Overall, the calibration results are reasonable. At most gage locations the numerical model results are in remarkable agreement with prototype data. In the region around G6 (Figure 11A and 11B), SG6 (Figure 12) and SG8 (Figure 13), large salinity gradients existed and salinity changed appreciably over relatively short distances. It is a very dynamic area due to its location relative to the main river inflow. The model results are improved by the addition of the horizontal density gradient terms. The most significant salinity variations occur near the exit of East Bay. For example, G6 (Figures 11A and 11B) is the gage station near the mouth of East Bay. Figure 11B shows the significant improvement after adding the horizontal density gradient terms. Two other gage stations (SG6 and SG8) are also near the exit of the East Bay. The "MODEL 2" results of these two gages (Figures 12 and 13) also match the prototype data very well. The two-layer hydrodynamic salinity model (with horizontal density gradient terms) is sufficient to illustrate this physical phenomenon, because this formulation couples the salinity equation and hydrodynamic equations through the density gradient terms.

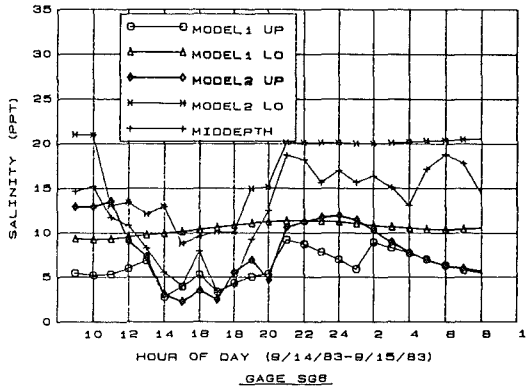

Figure 12. Salinity at Station SG6 for Calibration Condition.

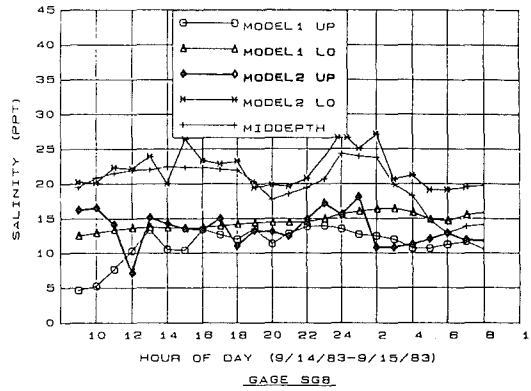

Figure 13. Salinity at Station SG8 for Calibration Condition.

Salinity contours, based on MODEL 1 and MODEL 2 results, are presented for both layers in Figures 14 thru 21 at low tide and high tide for the calibration period. The movement of the salinity contours over the calibration period appears consistent with the primary driving forces: tidal elevations and river inflow. At low tide (Figures 14 thru 17), the total river flow increased from 35,000 cfs to over 40,000 cfs and the higher salinity levels are pushed away from the fresh water inflow

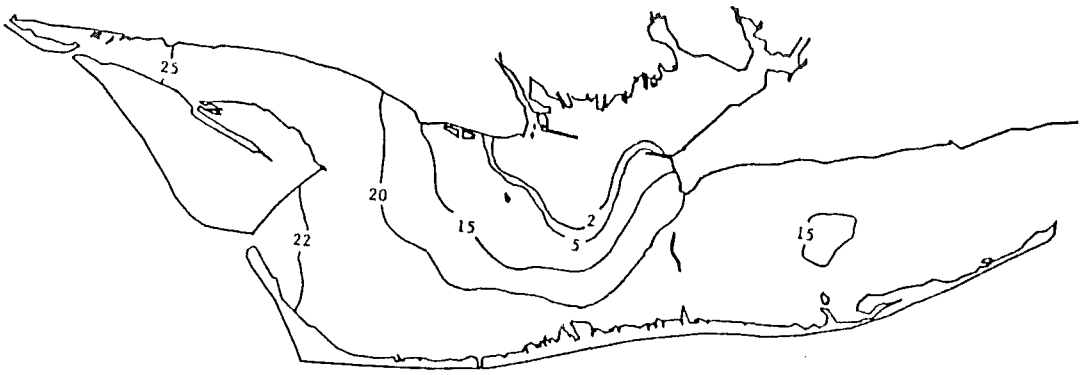

Figure 14. Salinity Contours of the Upper Layer at the Low Tide - Without Horizontal Density Gradient Terms.

Figure 15. Salinity Contours of the Lower Layer at the Low Tide - Without Horizontal Density Gradient Terms.

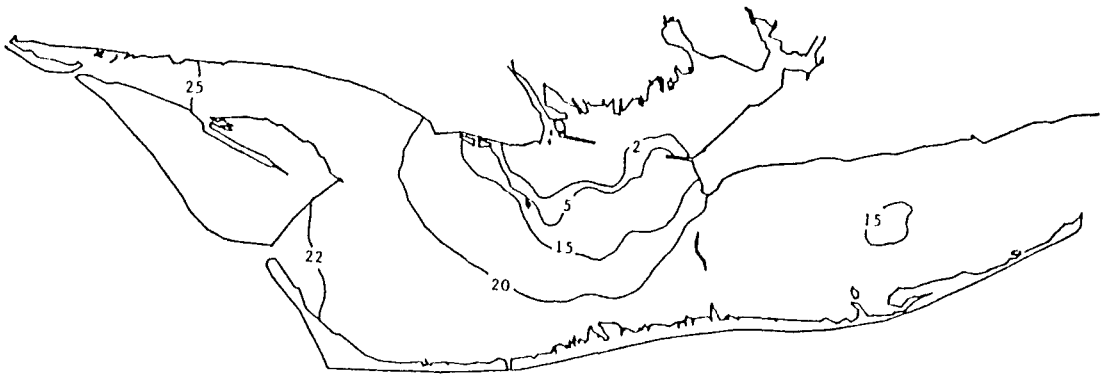

Figure 16. Salinity Contours of the Upper Layer at the Low Tide - With Horizontal Density Gradient Terms.

DOI: 10.18785/negs.1201.01

Figure 17. Salinity Contours of the Lower Layer at the Low Tide - With Horizontal Density Gradient Terms.

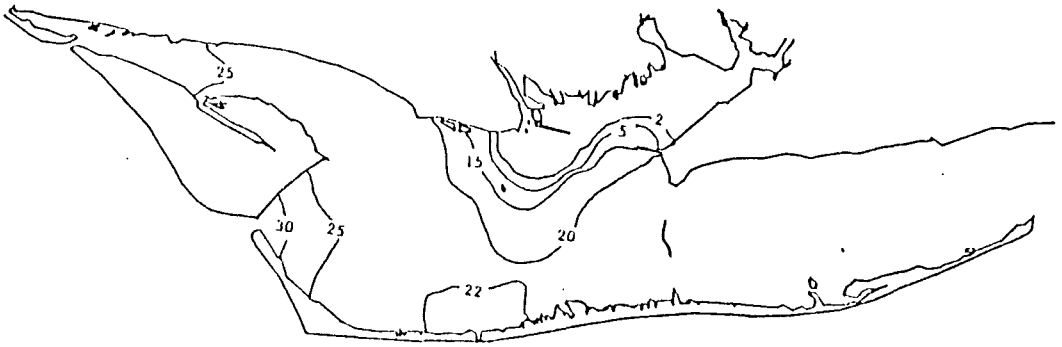

Figure 18. Salinity Contours of the Upper Layer at the High Tide - Without Horizontal Density Gradient Terms.

Figure 19. Salinity Contours of the Lower Layer at the High Tide - Without Horizontal Density Gradient Terms.

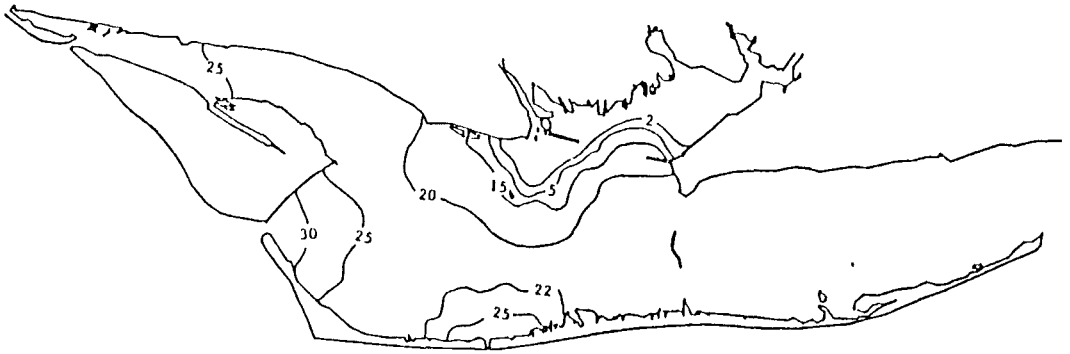

Figure 20. Salinity Contours of the Upper Layer at the High Tide - With Horizontal Density Gradient Terms.

Figure 21. Salinity Contours of the Lower Layer at the High Tide - With Horizontal Density Gradient Terms.

locations. Observe that the 2-5 ppt water was pushed completely out of East Bay of the upper layer (Figure 14). At high tide, the surface elevations in the bay increase, and the salinity contours reflect the movement of the higher salinity water back into areas near the fresh water inflow. Observe that the 2-5 ppt water of the upper layer has return to East Bay in Figures 18 and 20. Even the 10-15 ppt water of the lower layer has returned to East Bay at high tide, and the bay system has a relatively high salinity level with 10 to 15 ppt water extending up into some areas of East Bay in Figure 21.

The period March 8-9, 1984, was used as the verification condition. The basic model parameters established in the calibration process were fixed and only tide, wind, and river boundary conditions were changed for the verification run.

The surface elevation and velocity results are not changed significantly by the addition of the horizontal density gradient terms for the verification period. Surface elevation and velocity results are presented only for the without density gradient terms conditions. For example, Figure 22 presents the surface elevation without horizontal density gradient terms. Velocities without horizontal density gradient terms are presented in Figure 23.

Salinity results with and without horizontal density gradient terms are presented in Figures 24 thru 25. In many cases the salinity changes from 2 ppt to 10 or 15 ppt within a few thousand meters. In these regions very large salinity gradients exist. The addition of the horizontal density gradient terms produces significantly improved salinity results in regions of high salinity gradient. Results at SG8 (Figure 24), and G6 (Figure 25A and 25B) clearly illustrate the importance of the horizontal density gradient terms.

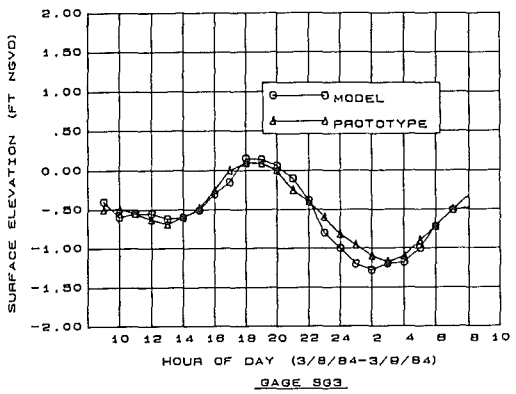

Figure 22. Surface Elevation at Station SG3 for Verification Condition.

DOI: 10.18785/negs.1201.01

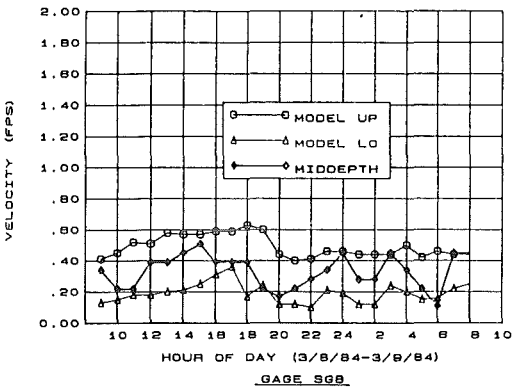

Figure 23. Velocity at Station SG8 for Verification Condition.

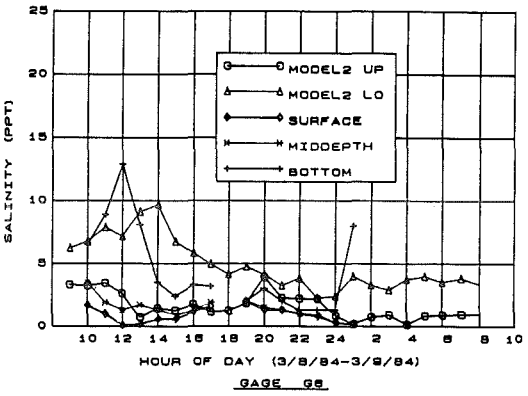

Figure 25B. Salinity at Station G6 of MODEL 2 for Verification Condition.

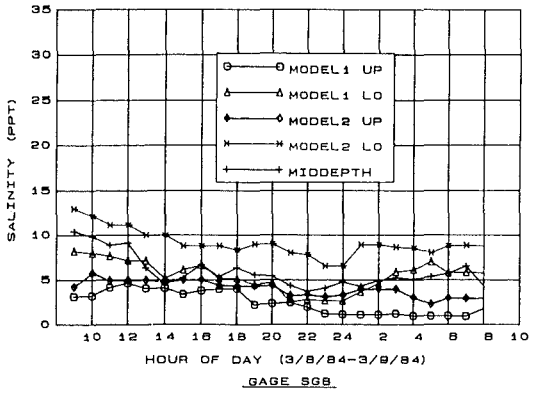

Figure 24. Salinity at Station SG8 for Verification Condition.

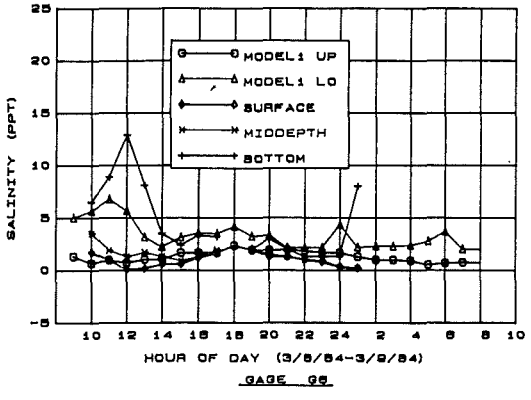

Figure 25A. Salinity at Station G6 of MODEL 1 for Verification Condition.

CONCLUSIONS AND DISCUSSION

This research has produced an improved two-layer hydrodynamic and salinity model for estuaries. The modeling results are the hydrodynamics and salinity distribution in an upper layer and in a lower layer of an estuary.

A theoretical approach to the internal wave boundary condition has been developed in a two-layer hydrodynamic and salinity model. An internal wave boundary conditions for the lower layer is based on modification of the surface elevation.

Horizontal density gradient terms have been introduced into the two-layer hydrodynamic salinity model formulation by approximating the density gradient in terms of salinity gradients. The horizontal density gradient terms represent an additional forcing term in the equation of motion. The hydrodynamic and salinity calculation in this model are coupled through the horizontal density gradient terms. This type formulation has not been done previously in two-layer models. In general, the density gradient terms are relatively small compared with the surface elevation gradient terms in most parts of the bay. However, in regions where large salinity changes occur, the

density gradient terms may locally be larger than the surface elevation gradient terms. Thus, while the region where density gradient terms predominate may be restricted, secondary effects produced by these terms may be significant throughout a large portion of the bay. Even in estuaries which may be relatively unstratified vertically, there will exist horizontal density or salinity gradients.

The two-layer model can offer more efficient results of physical details of the estuaries, and helpful information to deal with environmental consideration in estuaries. The two-layer model provides a compromise between the depth averaged model and the more complicated fully three-dimensional model.

LITERATURE CITED

Anderson, D.A., and J.C. Tannehill, and R.H. Pletcher. 1984. Computational Fluid Mechanics and Heat Transfer, McGRAW-HILL Book Company, New York, NY, 167-169.

Jin, K.R., and D.C. Raney. 1989. A Two-Layer Hydrodynamic Salinity Model. The Sixth Symposium on Coastal and Ocean Management, Charleston, South Carolina July 11-14, pp2754-2768.

Jin, K.R., and D.C. Raney. 1989. Internal Wave Boundary Condition for A Two-Layer Hydrodynamic Model. Proceedings of the 12th Canadian Congress of the Applied Mechanics, Ottawa, Ontario, Vol 2, 562-563.

Leendertse, J.J. 1970. A Water-Quality Simulation Model for Well-Mixed Estuaries and Coastal Seas. Vol. 1, Principals of Computation, RM-6230-RC, Rand Corporation, Santa Monica, CA.

Leendertse, J.J. 1971. A Water-Quality Simulation Model for Well-Mixed Estuaries and Coastal Seas. Vol. 2, Computation Procedures, R-708-NYC, Rand Corporation, New York.

Liu, S-K, and J.J. Leendertse. 1979. A Three-Dimensional Model for Estuaries and Coastal Seas: Vol. VI, Bristol Bay Simulations. R-2405-NOAA.

Pritchard, D.W. 1971. Estuarine Modeling: An assessment, NTIS Rep. PB-206807, Environmental Protection Agency, Washington, DC.

Raney, D.C., I. Huang, and H. Urgun. 1987. A Hydrodynamic and Salinity Model for Apalachicola Bay, Florida. Research Report No. 339-183, The University of Alabama Bureau of Engineering.

Raney, D.C., and K.R. Jin. 1988. Importance of Density Gradient Terms in Estuaries. Hydraulic Engineering Proceedings of the 1988 National Conference, Colorado Spring, Colorado, Published by ASCE, New York.

Roache, P.J. 1972. Computational Fluid Dynamics, Hermosa publishers, Albuquerque, NM, 15-204.

Smith, L.H. and R.T. Cheng. 1987. Tidal and Tidally Averaged Circulation Characteristics of Suisun Bay, California. Water Resources Research, 23(1), 143-155.

Van Der Kreeke, J. 1988. Dispersion in Shallow Estuaries, Chapter 3, Hydrodynamics of Estuaries, Vol. I, Estuarine Physics, edited by Bjorn Kjerfve, CRC Press Inc.

Vreugdenhil, C.B. 1979. Two-Layer Shallow-Water Flow in Two Dimensions, a Numerical Study. J. of Computational Physics, 33: 169-184.

Wanstrath, J.J., R.E. Whitaker, R.O. Reid, and A.C. Vastand. 1976. Storm Surge Simulation in Transformed Coordinates. Vol. 1 Theory and Application. Technical Report 76-3, U.S. Army Coastal Engineering Research Center, CE, Fort Belvoir, Virginia.

Yoshida, S. and M. Kashiwamura. 1976. Tidal response of two-layer flow at a river mouth. Proceedings of the 1976 Coastal Engineering, 183, 3189-3207.

DOI: 10.18785/negs.1201.01

APPENDIX — NOTATION

The following symbols are used in this paper:

- c : Chezy Coefficient
- c_d : Drag Coefficient
- D_x , D_y : Mixing Coefficent of the salt in x, y direction
- d : Total Depth of the Layer
- f : Coriolis Parameter
- g : Gravitational Acceleration
- h : Depth of the Layer
- K : Kinematic Eddy Viscosity
- k : Eddy Viscosity
- p : Pressure
- S : Salinity (A Measure of the Mass of Dissolved Salts in One Kilogram of Sea Water)
- t : Time
- U, V, W : Mean Velocity Components in the x, y, z Direction
- u, v, w : Velocity Components in the x, y, z Direction
- x, y, z : Rectangular Coordinate Variables
- η : Vertical Deviation of each layer
- ν : Coefficient of Interfacial Friction
- ρ : Density
- ρ_a : Density of Air
- ρ_w : Density of Fresh Water
- τ_{bottom} : Bottom Stress
- τ_{inter} : Interfacial Stress
- τ_{wind} : Wind Stress

Subscripts 1 and 2 represent the upper and lower layers.